Estimating reliable earth properties from simultaneous velocity and reflectivity inversion

Yang Yang[1*], Sriram Arasanipalai[1], Nizar Chemingui[1] and Nicholas Montevecchi[2] describe how a new simultaneous velocity and reflectivity inversion workflow can provide accurate and high-resolution attributes for better quantitative interpretation and reservoir analysis.

Introduction

Seismic attributes are widely used in hydrocarbon exploration and play a key role in prospect identification. Seismic inversion has typically been the solution to derive earth models, particularly velocity and reflectivity which are then used to calculate these attributes. Traditionally, a workflow using Full Waveform Inversion (FWI) followed by Least-Squares Reverse Time Migration (LS-RTM) has been employed to invert for subsurface velocity and reflectivity models. Recently, Yang *et al*. (2021) introduced a new scheme that combines both inversions into a single process. A key aspect of the new solution is the separation of the low- and high-wavenumber components of the earth model, enabling the inversion to simultaneously update the velocity and reflectivity with minimum crosstalk. The approach is equivalent to performing FWI and LS-RTM simultaneously, where both velocity and reflectivity are continuously updated at each iteration. The iterative inversion compensates for incomplete acquisitions and varying illumination in the subsurface to provide true-amplitude earth reflectivity. The high-fidelity velocity and reflectivity models are then readily available for Quantitative Interpretation (QI). Moreover, they are employed to derive additional earth attributes, mainly relative impedance and density for prospectivity assessment.

In this study, we demonstrate how simultaneous inversion can deliver reliable velocity and reflectivity models for interpretation using 3D seismic data from the Orphan and Salar Basins, offshore Newfoundland and Labrador, Canada. Also, we show how additional properties such as relative impedance and relative density can be estimated directly from the inverted models. With more reliable attributes, more insights on prospectivity can be obtained beyond the capabilities of conventional processing.

Methodology — Simultaneous inversion of velocity and reflectivity

In seismic inversion, FWI and LS-RTM share a similar framework, both aiming at the minimization of the misfit between modelled and recorded data. Accordingly, it is possible to solve both inversions in a joint scheme. The most common approach is to augment the solution with an additional Born modelling relation (Mora, 1989) that is based on a first-order approximation to perturbation theory. In our workflow, we use the acoustic wave equation parameterized in terms of velocity and vector reflectivity (Whitmore *et al*., 2020) by reformulating the variable density wave equation. With no approximation in this reformulation, our modelling relation can generate the full acoustic wavefield, including refracted and reflected energy as well as free-surface and internal multiples.

The velocity and the vector reflectivity are computed based on their appropriate kernels after scale separation and the

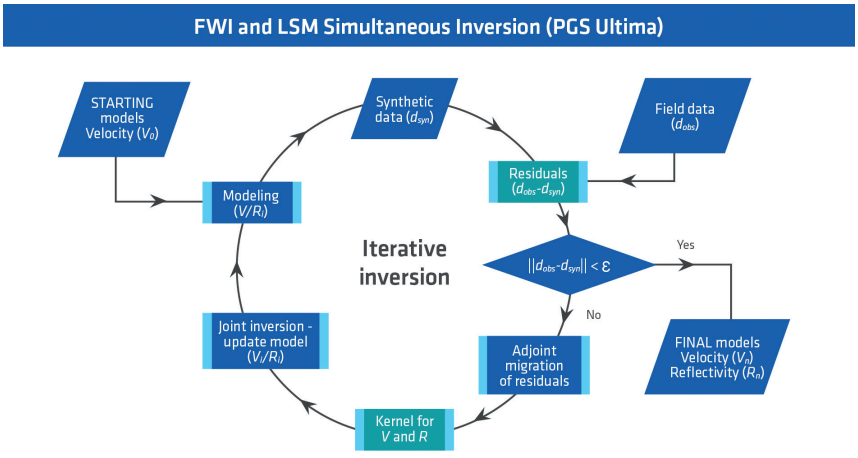

Figure 1 Simultaneous full waveform inversion workflow for velocity and reflectivity.

[1] PGS | [2] Oil and Gas Corporation of Newfoundland and Labrador
[*] Corresponding author, E-mail: yang.yang@pgs.com
DOI: 10.3997/1365-2397.fb2022103

inversion updates both parameters during each iteration. The inversion workflow is summarized in Figure 1. A starting velocity model is required for the inversion while an initial reflectivity is computed during the first iteration as an RTM image.

Application to shallow water survey — Blomidon 3D

The first study area for illustrating the benefits of our inversion method is in the Orphan Basin, offshore Newfoundland and Labrador, Canada (Figure 2). Tectonic history indicates that the basin has experienced two phases of rifting throughout the Jurassic and Cretaceous periods associated with the opening of the North Atlantic Ocean, followed by quiescent deposition within a passive margin setting throughout the Late Cretaceous and Cenozoic where basin architecture is dominated by thermal subsidence. As a result of the depositional and tectonic history, several key play types have been identified within the region ranging from predominantly structurally bound shore face plays in the Mid-Late Jurassic through turbidites and fan complexes throughout the Cenozoic. The Blomidon 3D survey is located on the present-day shelf to deep water transition, shows prospectivity throughout the sedimentary column. The Cenozoic section is anomalously thick and characterized by large marine shale units as well as Oligocene-aged fan complexes. These large-scale fans which rim the south and west margins of the Orphan Basin have sparked recent exploration interest in the region due to their size and insights from advanced geophysical interpretation.

The contributing 3D survey for this study was acquired in 2020 using multi-sensor streamer technology. This narrow azimuth data was acquired using 16 cables, 100 m streamer separation and 8-km streamer length. A smooth regional initial velocity model was used as a starting point for the inversion. The objective of this study was to build a reliable velocity model and to improve imaging of the Tertiary (~1 km to ~6 km) and ideally Jurassic sections (> ~6 km) (see Figure 3). A water column of 300 m with a high water-bottom reflectivity produces strong short-period multiples in the area of interest.

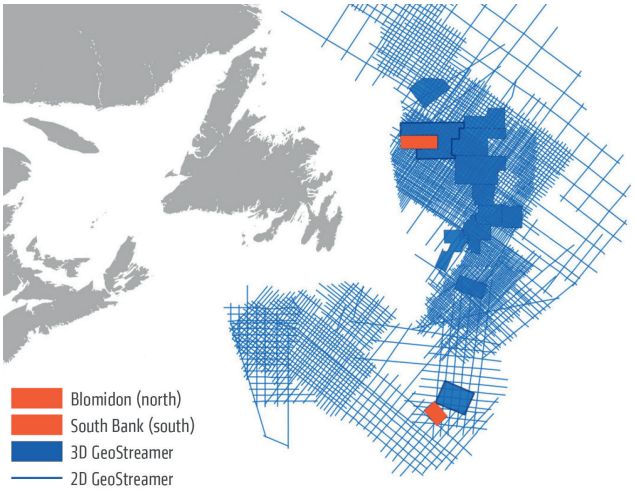

Figure 2 Map outlining the location of the two surveys used in this study: Blomidon 3D (north) and South Bank (south). Data was acquired with multi-sensor broadband technology.

Of particular interest for this study is a large-scale Oligocene fan complex, named the Jeffries prospect, identified directly below the present-day shelf and shelf break in shallow water. This juxtaposition of prospectivity and imaging challenges related to multiple suppression create a situation in which class II/IIp anomalies are not confidently interpretable. The uplift from simultaneous inversion progresses the understanding of such leads and prospects.

The maximum frequency used for the inversion in this first example is 20 Hz. The initial velocity model for the inversion was a time velocity model converted to depth. The background velocity has not been well resolved in the shelf due to multiple contamination in the model-building phase. Figure 3a shows the reflectivity from the first iteration of the inversion, which is equivalent to performing RTM with the initial model. In this

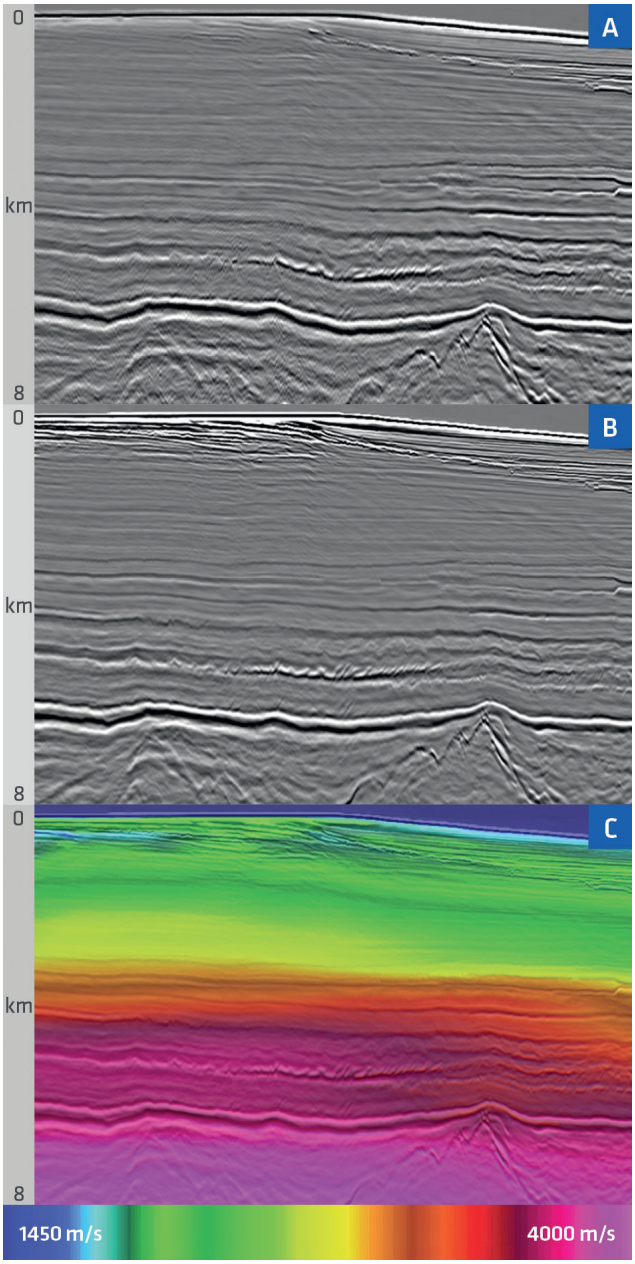

Figure 3 Orphan Basin field data example (a) The initial and (b) The final inverted reflectivity. (c) Inverted velocity model. Significant imaging improvements can be observed after inversion.

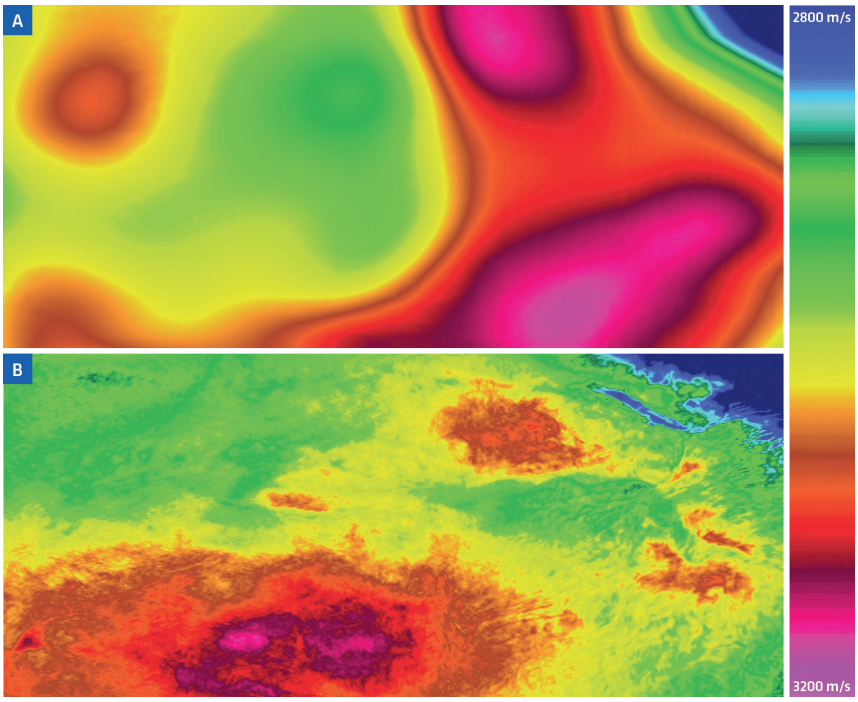

Figure 4 Depth slice at the target level from (a) Initial tomography velocity model and (b) Inverted velocity model from simultaneous inversion.

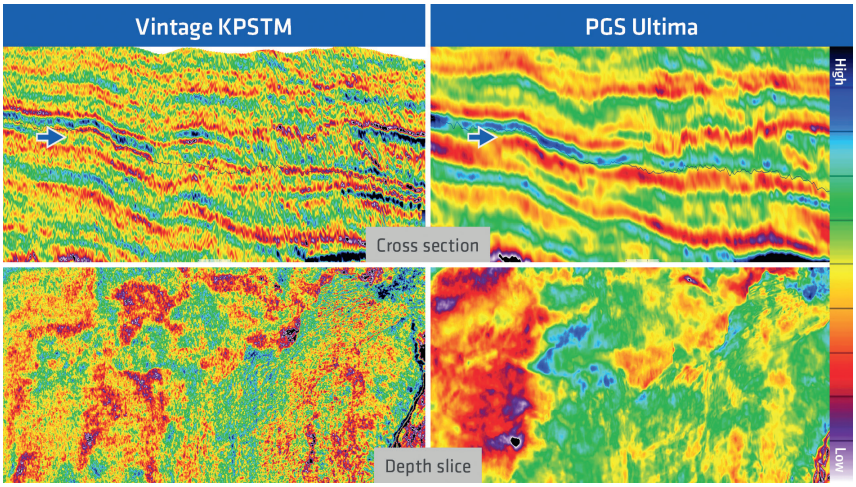

Figure 5 Comparison of the impedance model derived from vintage KPSTM and simultaneous inversion. Top: cross section display. Bottom is the depth slice display.

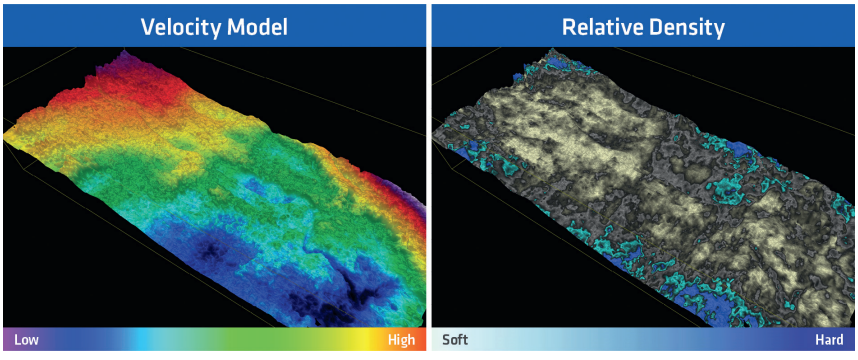

Figure 6 Velocity model and relative density model horizon extraction at the Jeffries lead from simultaneous inversion.

image, note the key areas in the Tertiary and rift sections that are not well imaged.

The results from the simultaneous inversion are shown in Figures 3b and 3c. The inverted velocity model shows significant improvement in the detail in the shallow section driven by the diving waves. The deeper sections are also geologically consistent after inversion, which is mainly achieved using reflection data. The inverted reflectivity shows better resolution and allows for better interpretation of the key lead and consequently a better understanding of the petroleum system.

Figure 4a and 4b display a depth slice of the initial model and the inverted velocity model from the simultaneous inversion. Enhanced resolution of the inverted velocity model better constrains the depth structures throughout the study area, which is

of particular importance in the shelf-to-slope transition. Velocity updates correct for structure misplacements between the initial and inverted reflectivity in the order of 200-300 m in some areas. Likewise, velocity updates change dip orientations on specific leads. In addition, the shallow velocity resolution improves the illumination problems observed deeper in the images obtained with the initial model. By combining the high-resolution velocity and the improved reflectivity models from the inversion, we are able to confirm the presence and enhance the ability to map anomalies in this shallow water scenario. Resolving these anomalies is critical to understanding the prospectivity, shallow hazards and DHIs.

Figure 5 shows an estimate of relative impedance model on a cross section (top) and depth slice (bottom) comparison between a PSTM AVA simultaneous inversion (conventional workflow) and the velocity-reflectivity simultaneous inversion (PGS Ultima). Traditionally, to estimate the relative impedance or elastic properties, AVA (Amplitude Versus Angle) simultaneous inversion is needed. In contrast, the simultaneous inversion workflow is totally data-driven and requires no special gather/angle conditioning and rock physics knowledge. The relative impedance/density can be solved directly from the definition of the inverted vector reflectivity. Although both results show similar trends and structures, it's clear that the relative impedance from simultaneous inversion presents better results for prospectivity analysis. In particular, the inversion boosts the signal-to-noise ratio significantly bringing significant benefits for QI analysis.

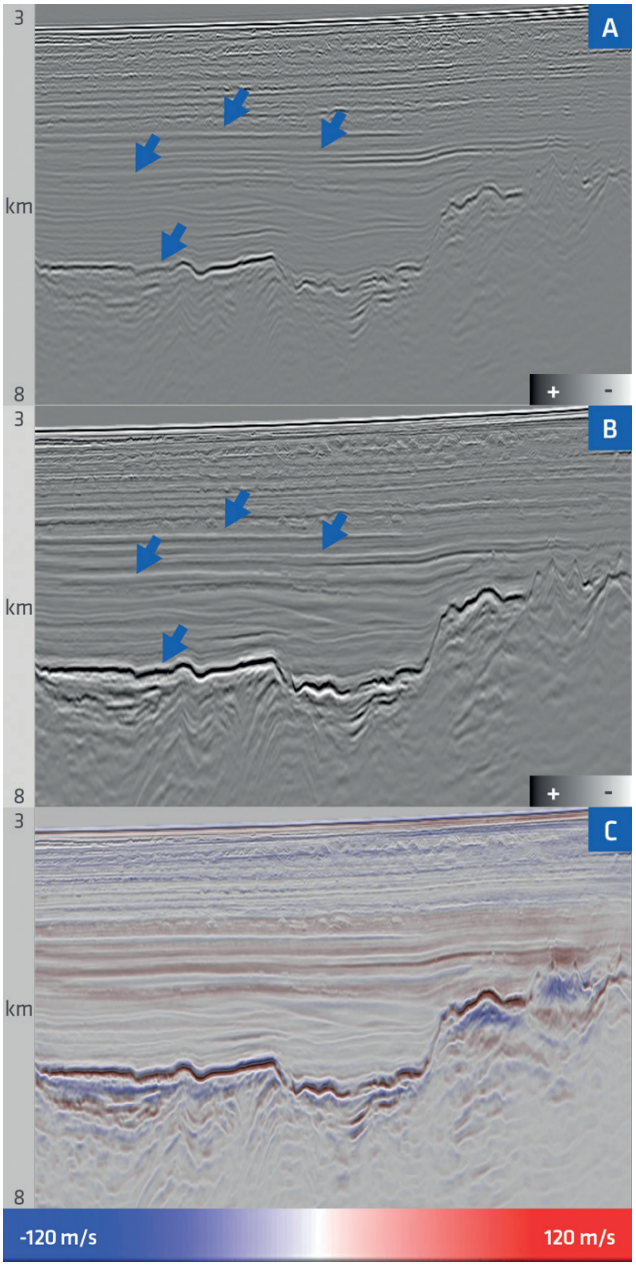

Figure 7 A subline section of the initilal reflecitivity (a) and the final inverted vertical reflectivity (b). (c) Final velocity updates from simultaneous inversion.

Inverted velocity and relative density attributes extracted at the target Jeffries Lead horizon are shown in Figure 6. The relative density estimate is structurally consistent and shows the potentially prospective (soft response) primary and secondary fan.

In addition to the improved individual lead evaluation demonstrated above, the inversion outputs provide better geological understanding via enhanced imaging and property constraints throughout the entire seismic section. The direct outputs of velocity and density produce constrained, layer-based properties for QI, while the reflectivity outputs are of significant interest as the inversion corrects for illumination issues created by limited acquisition and conventional imaging flows and thus reflects more accurately the true amplitudes of the sub-surface.

Application to deep water survey — South Bank

The second dataset, located at Salar Basin in southeast Newfoundland, is an early Cretaceous, isolated rift basin with passive margin fill from late Cretaceous period and onward. Many fan systems have been identified along the margin using existing seismic data. They are interpreted as Oligocene in age, and the main prospectivity is believed to lie in these fans originating from the shelf and shelf-edge deltas. Class II anomalies are observed in the reservoir interval, along with class IV responses in the deeper section analogous to a modelled source rock in the region.

The South Bank 3D survey was acquired in 2020 using multi-sensor streamer technology. This narrow azimuth data was also acquired using 16 cables, 100-m streamer separation and 8 km streamer length. The average water column depth is more than 3 km in this area. The objective of this study was to build a more-detailed higher-resolution velocity model and to better define the target fan system.

The inversion started from a smooth version of a tomographic velocity model. After simultaneous inversion the background model is further repaired, and more details are also added after simultaneous inversion.

An inline section of the reflectivity from the first iteration of the inversion is shown in Figure 7(a). This is equivalent to performing RTM using the initial velocity model. The final inverted reflectivity is displayed in Figure 7(b). It shows higher resolution, particularly in the shallow, and a broader bandwidth character after inversion. Amplitudes are better balanced across the section with better imaging of the steeply dipping structures in the deeper part of the section. A high-resolution velocity

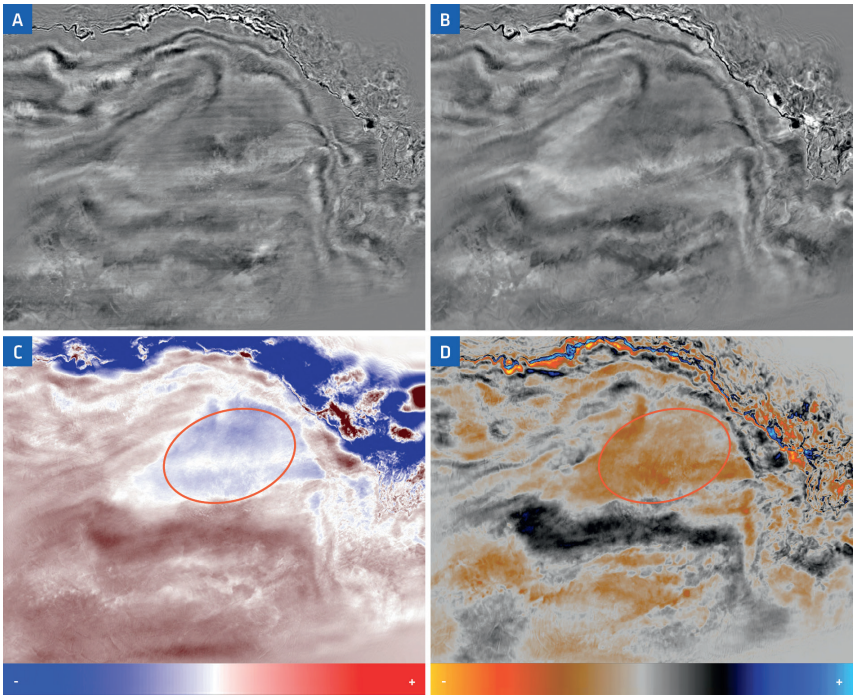

Figure 8 Depth slice extraction at the target fan system level for (a) Initial reflectivity, (b) Final inverted reflectivity, (c) Velocity updates and (d) derived relative density.

model and reflectivity cube are acquired at the same time from the simultaneous inversion. The velocity updates in Figure 7(c) illustrate the details recovered by the FWI on top of the smooth starting model. The background velocity models are also corrected for a more accurate reflector depth. The detailed velocity updates at the target level fan system show some structurally conformed updates, which provide important information for reservoir analysis.

Figure 8(a) and (b) show the initial and inverted reflectivity at the target reservoir level. In addition to the enhanced resolution and the balanced illumination, notice the attenuation of the sail-line footprint from the initial image through the inversion, leading to artifact-free attributes for QI. The velocity updates at the target level are shown in Figure 8(c). They illustrate a high level of detail and conformity with the structure. Similarly, the relative density derived from the inverted velocity and reflectivity is plotted in Figure 8(d) and shows good correlation with the latter earth properties. It is worth noting the drop in velocity and density in the prospect zone which provides valuable information about the potential reservoir. Such additional information is difficult to get from conventional workflows.

Discussion

The benefits of simultaneous inversion are demonstrated with the above two field data examples from Canada. Although the depth of the water column and the overall geology is quite different, significant improvement can be observed from the inversion result for both examples. The inversion utilizes the full acoustic wavefield through an alternative formulation of the wave-equation parametrized in terms of velocity and vector reflectivity. The reflectivity is updated while refining the velocity model. The nonlinear LS-RTM results show significant structural improvements, more focusing, and better fault imaging compared to the conventional migration. The results also deliver better amplitude fidelity and signal-to-noise ratio.

The simultaneous inversion takes advantage of the similarities between FWI and LS-RTM. The scale separation based on inverse scattering imaging condition updates the velocity and reflectivity with minimum crosstalk between the two models. Particularly, reflectivity changes caused by density variations are not erroneously mapped as velocity updates. Using the accurate inverted velocity and reflectivity models, we demonstrate that additional properties, namely relative impedance and relative density, can be estimated directly from the inverted models. Those attributes are important for prospectivity analysis and reservoir studies. Generation of such reliable attributes can be extremely difficult using traditional QI workflows. Thus, the inverted models and additional properties can be directly used to understand the petroleum system, reliably identify leads, and ultimately reduce exploration risk.

Conclusions

We applied a new inversion solution for simultaneous estimation of velocity and the earth's reflectivity to two datasets from offshore Canada. Results showed that while the background velocity model is iteratively updated, an accurate estimate of the earth reflectivity is simultaneously generated. The resulting images show higher amplitude fidelity and higher signal-to-noise ratio. The inverted models can be used to calculate additional properties such as relative density, which is useful for improving prospectivity analysis.

The simultaneous inversion products, i.e., velocity, reflectivity, and the derived relative impedance and density, besides improving individual lead evaluation, also provide better property constraints for QI and shallow anomaly interpretation. To this point, the technology assists in derisking potential prospectivity in areas with imaging challenges and produces markedly different

but more trustworthy results compared to conventional processing techniques.

The current implementation of the simultaneous inversion is based on stacked vector reflectivity. The next development step is to extend the inversion to generate angle gathers, which can provide more properties to help quantitative interpretation of potential hydrocarbon prospects.

Acknowledgements

The authors would like to thank PGS for permission to publish the paper and PGS Multi-Client for providing the data in this study. We would also like to thank Oil and Gas Corporation of Newfoundland and Labrador (OilCo) for their support.

References

Mora, P. [1989]. Inversion = migration + tomography, *Geophysics*, **54**(12), 1575-1586.

Whitmore, N.D., Ramos-Martinez, J., Yang, Y. and Valenciano, A.A. [2020]. Full wave field modeling with vector-reflectivity. 82nd EAGE Conference & Exhibition, Extended Abstracts, 1-5.

Yang, Y., Ramos-Martinez, J., Whitmore, N.D., Huang, G. and Chemingui, N. [2021]. Simultaneous inversion of velocity and reflectivity. *First Break,* **39**(12), 55-59.